Direct Observation of Magnon-Phonon Strong Coupling in Two-Dimensional Antiferromagnet at High Magnetic Fields

Sheng Liu,[1,*] Andrés Granados del Águila,[1,*] Dhiman Bhowmick,[1,*] Chee Kwan Gan,[2]
T. Thu Ha Do,[1] M. A. Prosnikov,[3] David Sedmidubský,[4] Zdenek Sofer,[4] Peter C. M. Christianen,[3]
Pinaki Sengupta,[1,†] and Qihua Xiong[5,6,‡]

[1]Division of Physics and Applied Physics, School of Physical and Mathematical Sciences,
Nanyang Technological University, Singapore 637371
[2]Institute of High Performance Computing, 1 Fusionopolis Way, 16-16 Connexis, Singapore 138632
[3]High Field Magnet Laboratory, HFML-EMFL, Radboud University, 6525 ED Nijmegen, Netherlands
[4]Department of Inorganic Chemistry, University of Chemistry and Technology Prague,
Technická 5, 166 28 Prague 6, Czech Republic
[5]State Key Laboratory of Low-Dimensional Quantum Physics and Department of Physics, Tsinghua University,
Beijing 100084, China
[6]Beijing Academy of Quantum Information Sciences, Beijing 100193, China

We report the direct observation of strong coupling between magnons and phonons in a two-dimensional antiferromagnetic semiconductor $FePS_3$, via magneto-Raman spectroscopy at magnetic fields up to 30 Tesla. A Raman-active magnon at 121 cm^{-1} is identified through Zeeman splitting in an applied magnetic field. At a field-driven resonance with a nearby phonon mode, a hybridized magnon-phonon quasiparticle is formed due to strong coupling between the two modes. We develop a microscopic model of the strong coupling in the two-dimensional magnetic lattice, which enables us to elucidate the nature of the emergent quasiparticle. Our polarized Raman results directly show that the magnons transfer their spin angular momentum to the phonons and generate phonon spin through the strong coupling.

Magnons and phonons are quantized collective excitations in quantum magnets—both obeying Bose Einstein statistics—representing energy quanta of spin waves and atomic vibrations, respectively. Magnonics, which utilizes the propagation of spin waves to realize high-frequency information storage and computation [1–3] is a rapidly growing research frontier based on magnon dynamics. Interest in this is primarily driven by the extremely low energy consumption in magnonic devices due to the absence of charge transport [2–7]. However, the generation of magnons is currently inefficient as it relies on conversion from uncontrollable thermal energy [5–8].

The interaction between magnons and phonons allows hybridization between magnetic and phononic resonances, which provides possible mechanisms to excite, manipulate, and detect magnons by coupling to phononic modes. Previous studies demonstrate that the ferromagnetic (FM) magnons, whose intrinsic resonant frequencies are in the GHz range, can couple to acoustic phonons and microwave radiation around the same wavelength [7,9–11]. Those couplings are greatly enhanced in low-dimensional FM structures (e.g., thin film and nanocrystal) with lower symmetry and larger specific surface area [9–13]. While FM magnononics has made rapid advances in the recent past, antiferromagnetic (AFM)-based magnon dynamics is

rapidly emerging as a superior next generation frontier in magnonics. On one hand, the AFM ground state is much more stable than FM domains which are usually sensitive to small electromagnetic disturbances [6,7,14]. On the other hand, AFM magnons have typical resonance in the THz range, exhibiting the potential to process information 3 orders of magnitude faster than FM magnonics [4,6,10,15–19]. The coupling of AFM magnons to phononic resonance is in the energy range of optical phonons, which so far have not been well understood.

The recent discovery of two-dimensional (2D) ferromagnets has expanded ferromagnetism to an atomically thin limit [20–22], which opens up the 2D regime for spintronics and magnonics [23–26]. Similarly, monolayer anitiferromagnetism has been realized in $FePS_3$ and its family MPX_3 (M = Mn, Ni, and Co; X = S and Se) [8,27–31]. The predominantly 2D nature of these Van der Waals magnets makes them ideal platforms for coupling magnons and phonons, as the system contains entirely surface spins at the 2D limit [20,21,32], and the amplitude of transverse optical (TO) phonons are enhanced along the out-of-plane direction [33,34]. In this Letter, we report the first direct observation of strong coupling between magnons and phonons in two-dimensional antiferromagnetic semiconductor $FePS_3$ at

high magnetic fields up to 30 Tesla. As the magnetic field tunes the magnon spectrum to resonance with its nearest (in energy) phonon, a hybridized magnon-phonon quasiparticle is formed. Magnon spin angular momentum is converted into phonon spin through strong coupling. Our results, complemented by microscopic modeling, elucidate the mechanism of magnon-phonon coupling and will be crucial to the development of AFM-based magnonic devices.

We have systematically investigated the magnetic dynamics of a quadrilayer $FePS_3$ sample through magneto-Raman scattering at high magnetic fields up to 30 T, and temperatures 4.2–120 K to explore the coupling between magnonic and phononic modes (schematically illustrated in Fig. 1(a) (for complete experimental details, see Supplemental Material, Notes 1 and 2 [35]). The magnetic moment carrying Fe atoms is arranged in a 2D hexagonal lattice with Ising-like spins oriented in the out-of-plane direction. Two sublattices of spin-up (red) and down (blue) sites form in-plane chains along the zigzag direction, respectively, which are antiferromagnetically coupled. Four Fe atoms (a_1, a_2, b_1, and b_2) in one yellow box constitute a new unit cell, resulting in a new 2D rectangle lattice [Fig. 1(d)]. The Néel temperature (T_N) of $FePS_3$ is around 116 K, which is indicated by the sharp drop of magnetic susceptibility [Fig. 1(b)].
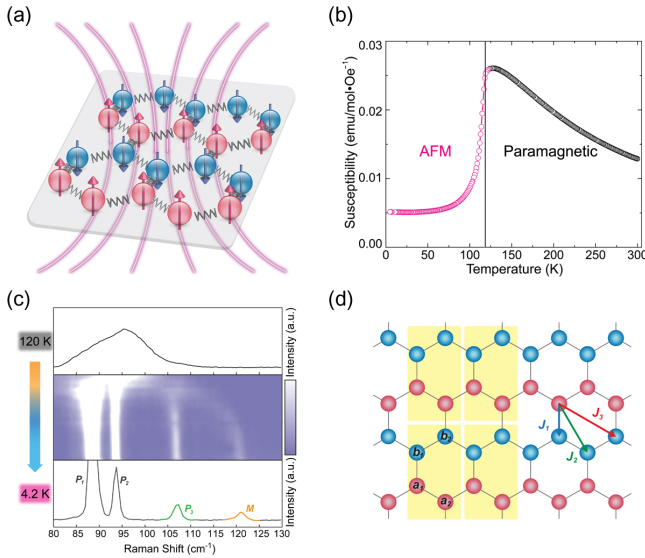

FIG. 1. (a) Schematic illustration of Fe moments coupled to lattice vibrational modes in $FePS_3$. (b) Temperature-dependent susceptibility of $FePS_3$ single crystal, showing Néel temperature $T_N \approx 116$ K. (c) Temperature-dependent Raman spectra of $FePS_3$ on SiO_2/Si substrate. A single broad peak at 120 K splits into 4 sharp peaks at 4.2 K. (d) 2D spin lattice of $FePS_3$ in AFM state. Each yellow box shows a unit cell. J_1, J_2, J_3 denote exchange coupling between first-, second-, and third-nearest neighbor Fe atoms.

Figure 1(c) shows the results of temperature-dependent Raman spectra on $FePS_3$. A Raman active magnon peak is identified at 121 cm^{-1} in the spectral range 80–140 cm^{-1} at 120 K (the full spectrum can be found in Supplemental Material, Note 2 [35]). The 2D contour plot displays spectral evolution from 120 K (upper spectrum) to 4.2 K (bottom spectrum). The broad Raman band evolves into three sharp Lorentz peaks, P_1, P_2 (gray), and P_3 (green) as temperature decreases to below T_N, which have been identified as signatures of the AFM phase transition [27–30]. The peak intensities increase rapidly as temperature decreases further, without any change of peak position. An AFM induced Brillouin zone folding is believed to be the most plausible reason behind the origin of these three peaks [27–29]. Interestingly, a much weaker peak M (orange) emerges at the higher wave number side of P_3. The zero-field position of M at 121 cm^{-1} is in good agreement with the resonance energy (~ 15 meV) obtained from inelastic neutron scattering measurement [46] and a recent Raman result[31]. The position of M blueshifts quadratically with decreasing T.

Next, the evolution of the Raman spectrum of $FePS_3$ in an out-of-plane magnetic field is investigated. The experimental results are summarized in Fig. 2(a). P_1, P_2, and P_3 have no energy shift with (low) magnetic field or temperature, and are therefore verified as phonons [31,47,48]. In contrast, the peak M exhibits a Zeeman splitting, confirming its magnonic character [49]. We label the two split peak sections as $M_\uparrow$ (red) and $M_\downarrow$ (blue) with opposite spins ($S_Z = \pm 1$).

At fields below 10 T, $M_\uparrow$ ($M_\downarrow$) redshifts (blueshifts) symmetrically, while P_1, P_2, and P_3 remain unchanged. For quantitative analyses, their spectral positions are extracted and shown in Fig. 2(b). The peak positions of $M_\downarrow$ (blue down triangles) and $M_\uparrow$ (red up triangles) show linear dependence on a magnetic field with similar slopes (0.99 and -0.94 cm^{-1}/T), which can be regarded as the effective g factor of the magnon (g_m). As the field further increases (> 10 T), $M_\downarrow$ keeps blueshifting linearly. However, $M_\uparrow$ stops redshifting as it approaches P_3 (green diamonds) instead of merging and crossing the P_3 curve. Interestingly, P_3 starts redshifting as $M_\uparrow$ stops. This nonlinear energy dispersion is fitted (solid lines) with a microscopic model that will be explained later. Until 22.5 T, the shift of P_1 and P_2 is negligible (some shifting happens at fields close to 30 T that will be discussed later). The field-driven anticrossing of $M_\uparrow$ and P_3 with a 6.1 cm^{-1} energy gap signals a repulsive interaction between the magnon ($M_\uparrow$) and phonon (P_3) modes when their energies are in resonance, which is evidence that the two modes are strongly coupled.

To uncover the mechanism behind the magnon-phonon strong coupling, we first analyze the magnon spectrum of $FePS_3$. The spin Hamiltonian capturing the magnetic behavior consists of Fe moments arranged in a honeycomb lattice:
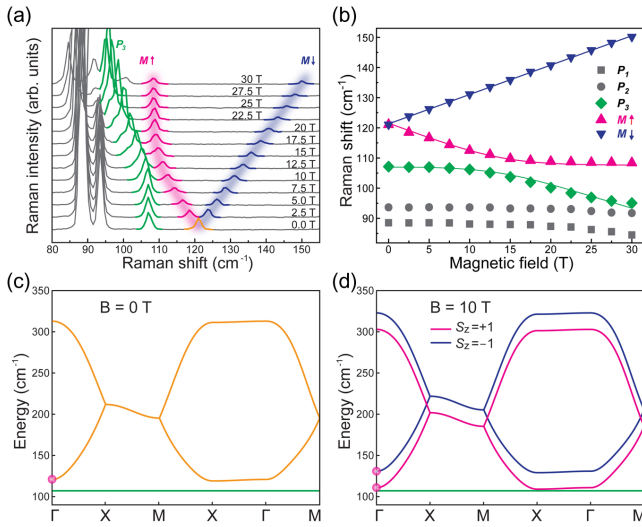
FIG. 2. (a) Raman spectra of $FePS_3$ in magnetic field 0 to 30 T. Raman spectra have been vertically shifted for clarity, in steps of 2.5 T. Zeeman splitting of the M branch identifies it as magnon mode. The two branches are denoted as $M_\uparrow$ (red) and $M_\downarrow$ (blue). (b) Magnetic-field-dependent peak position of P_1, P_2, P_3, $M_\uparrow$, and $M_\downarrow$, which are denoted as black squares, black circles, green diamonds, red up-triangles, and blue down-triangles. The solid lines are fits to the data. Calculated magnon dispersion diagrams at (c) 0 and (d) 10 T. The red dots on the magnon dispersion curves at Γ point denote Raman active modes. The green horizontal lines denote calculated phonon energy of P_3 at Γ point.

$$
\mathcal{H} = J_1 \sum_{\langle i,j \rangle} \hat{\mathbf{S}}_i \cdot \hat{\mathbf{S}}_j + J_2 \sum_{\langle\langle i,j \rangle\rangle} \hat{\mathbf{S}}_i \cdot \hat{\mathbf{S}}_j + J_3 \sum_{\langle\langle i,j \rangle\rangle} \hat{\mathbf{S}}_i \cdot \hat{\mathbf{S}}_j
$$
$$
+ \Delta \sum_i (S_i^z)^2 - g\mu_B B_z \sum_i S_i^z, \qquad (1)
$$

where $\hat{\mathbf{S}}_i$ is a Fe-spin at site i. The first three terms represent a Heisenberg interaction between first-, second-, and third-nearest neighbors; the fourth term denotes an easy-axis (Ising-type) anisotropy; and the last term represents a Zeeman energy due to an out-of-plane magnetic field B_z along the easy axis. The Hamiltonian parameters are determined from first principle calculations (see Supplemental Material Note 3 for details). The ground state of $FePS_3$ has an AFM order below T_N. The magnons are quasiparticle excitations above the ground state. We use the Holstein-Primakoff transformation to define the magnons on the up- and down-spin sublattices: $S_i^+ = \sqrt{2S}a_i$, $S_i^z = S - a_i^\dagger a_i$ (up-spin) and $S_j^+ = -\sqrt{2S}b_j$, $S_j^z = -S + b_j^\dagger b_j$ (down-spin), where $a_i^\dagger$ and $b_j^\dagger$ create a magnon on the respective sublattices. The Holstein-Primakoff transformation maps (1) to an effective tight binding magnon Hamiltonian, treating any interaction term in the mean field approximation. The magnon band structure is shown in Fig. 2(c). In the absence of an external field, the spectrum consists of two doubly degenerate bands.

The magnon band has two branches at the Γ point. Based on the magnetic point group, the higher energy magnon belongs to representation B_u which is Raman inactive. The lower energy magnon is the Raman-active A_g mode, whose Raman tensor is given as (see full derivation in Supplemental Material, Note 4 [35])

$$
R = \begin{pmatrix} I & iG & 0 \\ iC & A & 0 \\ 0 & 0 & E \end{pmatrix}. \qquad (2)
$$

Choosing $J_1 = 1.49$ meV, $J_2 = 0.04$ meV, $J_3 = -0.6$ meV, and $\Delta = -3.6$ meV [30,46], the Raman-active magnon is found to be in excellent agreement with M at 121.5 cm^{-1}— the Raman-inactive magnon is absent in our results (Supplemental Material, Fig. S1). Using experimentally obtained $g_{\mu_B} = g_m/8.066$ meV/T, the splitting of the magnon bands in a field can be calculated. Figure 2(d) shows magnon dispersion at 10 T, where $\mathcal{H}_{S_z=+1}$ (red curve) and $\mathcal{H}_{S_z=-1}$ (blue curve) subbands split, corresponding to $M_\uparrow$ and $M_\downarrow$. The green horizontal lines in Fig. 2(c) and 2(d) indicate the calculated phonon energy of P_3 at Γ point ($\sim$107.6 cm^{-1}), which has no field dependence. At this field, the magnon subband $\mathcal{H}_{S_z=+1}$ approaches the phonon (P_3), resulting in a hybridization of the two.

Next we present a qualitative microscopic picture of the two modes (M and P_3) in order to formulate a quantitative description of the hybridization between the two. At the atomic level, $M_\uparrow$ can be regarded as a superposition of two magnon holes (absence of magnon) at the spin-up sites and two magnons at spin-down sites in a unit cell. ($M_\downarrow$ is in the opposite configuration). The magnetic field parallel to the spin-up direction reduces the excitation energy for annihilation (creation) of magnon at spin-up (down) sites, causing the redshift of $M_\uparrow$. Considering a classical picture shown in Fig. 3(a), the hole magnon and magnon in $M_\uparrow$ can be viewed as spin precession ($\vec{M}_a$ and $\vec{M}_b$) about the magnetization direction (z axis). The torque on magnon $\vec{M}_b$ is greater than that of hole magnon $\vec{M}_a$. The phonon mode P_3 appears only in the AFM phase [Fig. 1(c)]. Similar phonon modes emerging in the AFM phase in the MPX_3 family have been proved to be associated to the magnetic atoms, i.e., Fe, Mn, and Ni [28,29,48,52–54]. Based on our first principle calculations, P_3 is visually depicted as Fe atoms at (a_1, b_1) and (a_2, b_2) sites vibrating oppositely in the out-of-plane direction forming a magnetoelastic oscillator (Supplemental Material Note 5). This provides a microscopic picture to model the magnon-phonon coupling—illustrated in Fig. 3(a)—at a high field (> 10 T) where the frequency of $M_\uparrow$ is in resonance with P_3.

In view of the above, the magnon-phonon strong coupling can be modeled based on single-ion magnetostriction on

each Fe site of the unit cell (a_1, a_2, b_1, and b_2) (see details of the modeling in Supplemental Material, Note 6 [35]). The magnetoelastic coupling Hamitonian is given as

$$\mathcal{H}_c = -\kappa\epsilon^{yz}(S_f^x S_f^z + S_f^z S_f^x) - \kappa\epsilon^{xz}(S_f^y S_f^z + S_f^z S_f^y), \quad (3)$$

where ϵ^{yz} and ϵ^{xz} are the strain functions to convert the in-plane strain to the out-of-plane direction. κ is the magnetoelastic coupling constant. The energy dispersion when $M_\uparrow$ and P_3 are strongly coupled is given by (Supplemental Material Note 6)

$$\omega^\pm = \frac{\omega_{M_\uparrow} + \omega_{ph}}{2} \pm \frac{1}{2}[(\omega_{M_\uparrow} - \omega_{ph})^2 + 4|M_c|^2]^{1/2}, \quad (4)$$

where ω^+ and ω^- describe the energy dispersion of the two anticrossing bands caused by strong coupling of magnons and phonons. $\omega_{M_\uparrow}$ and ω_{ph} are the frequencies of the magnons and phonons, respectively. M_c is the coupling matrix which includes eigenvectors and parameters from a previous calculation of magnon energies (Supplemental Material Note 4).

The characteristic equation (4) reproduces perfectly the experimentally observed field dependence of $M_\uparrow$ and P_3 peaks [Fig. 2(b)], with coupling strength $|M_c| \approx$ 2.93 cm^{-1} (87.8 GHz), which is at least 2 orders larger than the recent report of the FM magnon [11] (see details in Supplemental Material Note 6). The optimized model is plotted in Fig. 3(b), with red (green) denoting magnonlike (phononlike) behavior. The model shows three distinct regimes of the energy dispersion. At low fields (< 10 T), the lower (upper) band is predominantly magnonic (phononic) in nature that are only weakly coupled. From fields in the range 10–20 T, the magnon and phonon modes are strongly coupled to form a new quasiparticle. At a high field (> 20 T), the bands again have purely phononic and magnonic character, but their ordering is switched.

To further probe the nature of magnon-phonon strong coupling, we measured circular-polarization-resolved Raman spectra of FePS$_3$ with varying magnetic field. For left-handed excitation (σ^+) which correlates to the external field direction, Fig. 3(c) summarizes the observed polarized spectra at 0, 5, and 15 T (top to bottom panels). At zero field, M and P_3 show opposite polarization. At 5 T, the Zeeman-split $M_\uparrow$ and $M_\downarrow$ branches inherit the same polarization from M, whereas the polarization of P_3 remains unchanged. Interestingly, at 15 T $M_\uparrow$ and P_3 reverse their polarization. $M_\downarrow$, P_1, and P_2 that are not involved in the strong coupling show no change in polarization with varying magnetic field. Figure 3(d) plots the degree of circular polarization (DCP) for P_3, $M_\uparrow$, and $M_\downarrow$ vs the magnetic field. The DCP is defined as $(I_{\sigma^+} - I_{\sigma^-})/(I_{\sigma^+} + I_{\sigma^-}) \times 100\%$, where I_{σ^+} and I_{σ^-} are Raman intensity from left- and right-handed detection, respectively. At small fields, $M_\uparrow$ and $M_\downarrow$ have positive
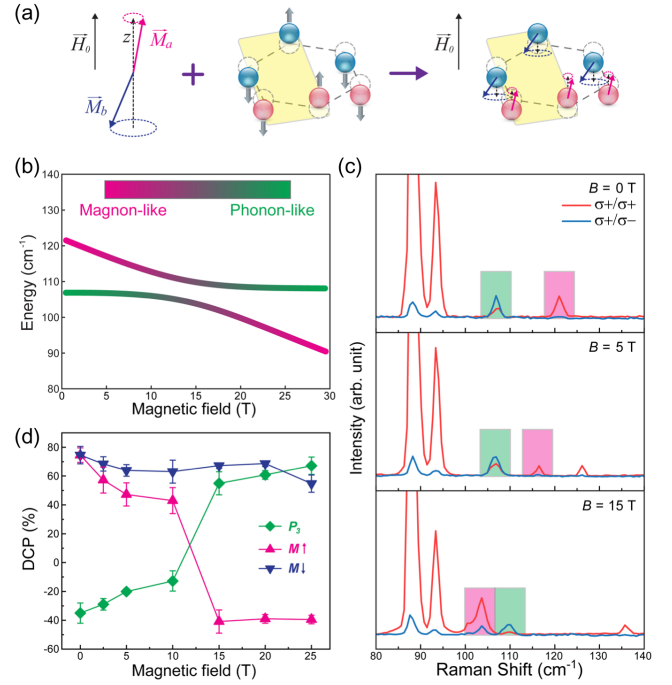

FIG. 3. (a) Schematic of magnon ($M_\uparrow$), phonon (P_3), and the magnon-phonon strong coupling in a classical description in FePS$_3$. (b) Simulation of the magnon-phonon strong coupling driven by magnetic field. Red (green) indicates magnonlike (phononlike) behavior. (c) Circular-polarization-resolved Raman spectra of FePS$_3$. The upper, intermediate, and bottom spectra are taken at 0, 5, and 15 T. Spectra in red and blue indicate copolarization and cross-polarization, respectively. (d) Magnetic-field-dependent DCP of P_3 (green), $M_\uparrow$ (red), and $M_\downarrow$ (blue). The DCP of P_3 and $M_\uparrow$ exchange after strong coupling occurs, while that of $M_\downarrow$ remains unchanged.

DCP, while P_3 shows negative DCP. With increasing field and onset of strong coupling, the DCP of $M_\uparrow$ and P_3 cross each other and change signs, resulting in reversed helicity for each of them. The DCP of $M_\downarrow$ remains unchanged all the time.

In the presence of a magnetic field, symmetries of the 2D spin lattice, and consequently, that of the Raman tensor remain the same as long as the AFM phase is sustained—destruction of the spin order at high fields could restore the Brillouin zone folding and alter the Raman spectra [27–29]. This is seen in the considerable redshift and intensity suppression of P_1 and P_2 when the field exceeds 22.5 T (Supplemental Material Note 7), which implies possible transition to the fully polarized state. The result provides critical information on limitations and magnetic ordering of the 2D antiferromagnet in a high magnetic field, which is worth future investigation under a field higher than 30 T.

Although $M_\uparrow$ and $M_\downarrow$ carry opposite spins [55,56], they inherit the same Raman tensor from M (opposite spins still cause electrical polarizability in the same direction).

The spin of $M_\uparrow$ is transferred to the TO phonon P_3 via the strong coupling and conservation of momentum [10,56,57], as illustrated in Fig. 3(a). The transfer of spin to the phonon can well explain the positive DCP of P_3 after strong coupling. Previously, similar spin of acoustic phonon has been demonstrated via coupling to the FM magnon which is a natural single mode with one chirality [10,51].

It is worthwhile to mention, when the degenerate magnon M shifts toward P_3 with increasing temperature, the two peaks merge without any sign of repulsion [see Fig. 1(c) and Supplemental Material, Fig. S11]. In this scenario, coupling does not occur because the shift of M stems from energy renormalization of the magnon band caused by enhanced magnon-magnon interaction (Supplemental Material Note 8). The thermal energy increases the density of magnons, making the magnon-magnon interaction much more prominent than the magnon-phonon interaction.

In conclusion, by applying a magnetic field in an out-of-plane direction of two-dimensional antiferromagnet FePS$_3$, we identify a magnon band directly in the Raman spectra. The magnon band splits into two degenerate magnon modes corresponding to opposite spin. At high field > 10 T, strong coupling between the $S_{z=+1}$ magnon subband and its adjacent phonon mode has been directly observed through the anticrossing of Raman peaks. A single-ion magnetostriction-based magnetoelastic Hamiltonian is built to successfully model the strong coupling. The derived energy dispersion fits the experimental data with high accuracy, which unambiguously confirms the observation of magnon-phonon strong coupling in a 2D antiferromagnet. Through the strong coupling, the magnon subband converts its spin to the phonon, generating phonon spin. In addition, as a semiconductor, FePS$_3$ preserves optoelectronic properties. Our finding highlights the potential of the 2D antiferromagnetic semiconductor as a hub system to integrate optoelectronic, phononic, and magnonic devices.

[*]These authors contributed equally to this work.
[†]psengupta@ntu.edu.sg
[‡]qihua_xiong@tsinghua.edu.cn

[1] V. Kruglyak, S. Demokritov, and D. Grundler, Magnonics, J. Phys. D **43**, 264001 (2010).

[2] Y. Kajiwara, K. Harii, S. Takahashi, J.-i. Ohe, K. Uchida, M. Mizuguchi, H. Umezawa, H. Kawai, K. Ando, and K. Takanashi, Transmission of electrical signals by spin-wave interconversion in a magnetic insulator, Nature (London) **464**, 262 (2010).

[3] A. V. Chumak, V. I. Vasyuchka, A. A. Serga, and B. Hillebrands, Magnon spintronics, Nat. Phys. **11**, 453 (2015).

[4] R. Lebrun, A. Ross, S. A. Bender, A. Qaiumzadeh, L. Baldrati, J. Cramer, A. Brataas, R. A. Duine, and M. Kläui, Tunable long-distance spin transport in a crystalline antiferromagnetic iron oxide, Nature (London) **561**, 222 (2018).

[5] Y. Wang, D. Zhu, Y. Yang, K. Lee, R. Mishra, G. Go, S. H. Oh, D. H. Kim, K. Cai, E. Liu, S. D. Pollard, S. Shi, J. Lee, K. L. Teo, Y. Wu, K. J. Lee, and H. Yang, Magnetization switching by magnon-mediated spin torque through an antiferromagnetic insulator, Science **366**, 1125 (2019).

[6] H. Fulara, M. Zahedinejad, R. Khymyn, A. A. Awad, S. Muralidhar, M. Dvornik, and J. Åkerman, Spin-orbit torque-driven propagating spin waves, Sci. Adv. **5**, eaax8467 (2019).

[7] J. Han, P. Zhang, J. T. Hou, S. A. Siddiqui, and L. Liu, Mutual control of coherent spin waves and magnetic domain walls in a magnonic device, Science **366**, 1121 (2019).

[8] W. Xing, L. Qiu, X. Wang, Y. Yao, Y. Ma, R. Cai, S. Jia, X. C. Xie, and W. Han, Magnon Transport in Quasi-Two-Dimensional van der Waals Antiferromagnets, Phys. Rev. X **9**, 011026 (2019).

[9] M. Weiler, L. Dreher, C. Heeg, H. Huebl, R. Gross, M. S. Brandt, and S. T. B. Goennenwein, Elastically Driven Ferromagnetic Resonance in Nickel Thin Films, Phys. Rev. Lett. **106**, 117601 (2011).

[10] J. Holanda, D. S. Maior, A. Azevedo, and S. M. Rezende, Detecting the phonon spin in magnon-phonon conversion experiments, Nat. Phys. **14**, 500 (2018).

[11] C. Berk, M. Jaris, W. Yang, S. Dhuey, S. Cabrini, and H. Schmidt, Strongly coupled magnon-phonon dynamics in a single nanomagnet, Nat. Commun. **10**, 2652 (2019).

[12] S. Neusser and D. Grundler, Magnonics: Spin waves on the nanoscale, Adv. Mater. **21**, 2927 (2009).

[13] C. Safranski, I. Barsukov, H. K. Lee, T. Schneider, A. A. Jara, A. Smith, H. Chang, K. Lenz, J. Lindner, Y. Tserkovnyak, M. Wu, and I. N. Krivorotov, Spin calori-tronic nano-oscillator, Nat. Commun. **8**, 117 (2017).

[14] S. Jiang, J. Shan, and K. F. Mak, Electric-field switching of two-dimensional van der Waals magnets, Nat. Mater. **17**, 406 (2018).

[15] P. Němec, M. Fiebig, T. Kampfrath, and A. V. Kimel, Antiferromagnetic opto-spintronics, Nat. Phys. 14, 229 (2018).

[16] M. A. Prosnikov, A. N. Smirnov, V. Y. Davydov, R. V. Pisarev, N. A. Lyubochko, and S. N. Barilo, Magnetic dynamics and spin-phonon coupling in the antiferromagnet Ni_2NbBO_6, Phys. Rev. B 98, 104404 (2018).

[17] S. F. Maehrlein, I. Radu, P. Maldonado, A. Paarmann, M. Gensch, A. M. Kalashnikova, R. V. Pisarev, M. Wolf, P. M. Oppeneer, J. Barker, and T. Kampfrath, Dissecting spin-phonon equilibration in ferrimagnetic insulators by ultrafast lattice excitation, Sci. Adv. 4, eaar5164 (2018).

[18] K. Olejník, T. Seifert, Z. Kašpar, V. Novák, P. Wadley, R. P. Campion, M. Baumgartner, P. Gambardella, P. Nemec, J. Wunderlich, J. Sinova, P. Kužel, M. Müller, T. Kampfrath, and T. Jungwirth, Terahertz electrical writing speed in an antiferromagnetic memory, Sci. Adv. 4, eaar3566 (2018).

[19] S. M. Rezende, A. Azevedo, and R. L. Rodríguez-Suárez, Introduction to antiferromagnetic magnons, J. Appl. Phys. 126, 151101 (2019).

[20] B. Huang, G. Clark, E. Navarro-Moratalla, D. R. Klein, R. Cheng, K. L. Seyler, D. Zhong, E. Schmidgall, M. A. McGuire, D. H. Cobden et al., Layer-dependent ferromagnetism in a van der waals crystal down to the monolayer limit, Nature (London) 546, 270 (2017).

[21] C. Gong, L. Li, Z. Li, H. Ji, A. Stern, Y. Xia, T. Cao, W. Bao, C. Wang, Y. Wang et al., Discovery of intrinsic ferromagnetism in two-dimensional van der Waals crystals, Nature (London) 546, 265 (2017).

[22] Z. Fei, B. Huang, P. Malinowski, W. Wang, T. Song, J. Sanchez, W. Yao, D. Xiao, X. Zhu, A. F. May et al., Two-dimensional itinerant ferromagnetism in atomically thin Fe_3GeTe_2, Nat. Mater. 17, 778 (2018).

[23] D. Zhong, K. L. Seyler, X. Linpeng, R. Cheng, N. Sivadas, B. Huang, E. Schmidgall, T. Taniguchi, K. Watanabe, M. A. McGuire et al., Van der Waals engineering of ferromagnetic semiconductor heterostructures for spin and valleytronics, Sci. Adv. 3, e1603113 (2017).

[24] T. Song, X. Cai, M. W.-Y. Tu, X. Zhang, B. Huang, N. P. Wilson, K. L. Seyler, L. Zhu, T. Taniguchi, K. Watanabe et al., Giant tunneling magnetoresistance in spin-filter van der Waals heterostructures, Science 360, 1214 (2018).

[25] W. Chen, Z. Sun, Z. Wang, L. Gu, X. Xu, S. Wu, and C. Gao, Direct observation of van der Waals stacking–dependent interlayer magnetism, Science 366, 983 (2019).

[26] N. Sivadas, S. Okamoto, X. Xu, C. J. Fennie, and D. Xiao, Stacking-dependent magnetism in bilayer CrI_3, Nano Lett. 18, 7658 (2018).

[27] T. Sekine, M. Jouanne, C. Julien, and M. Balkanski, Light-scattering study of dynamical behavior of antiferromagnetic spins in the layered magnetic semiconductor $FePS_3$, Phys. Rev. B 42, 8382 (1990).

[28] X. Wang, K. Du, Y. Y. F. Liu, P. Hu, J. Zhang, Q. Zhang, M. H. S. Owen, X. Lu, C. K. Gan, P. Sengupta et al., Raman spectroscopy of atomically thin two-dimensional magnetic iron phosphorus trisulfide ($FePS_3$) crystals, 2D Mater. 3, 031009 (2016).

[29] J.-U. Lee, S. Lee, J. H. Ryoo, S. Kang, T. Y. Kim, P. Kim, C.-H. Park, J.-G. Park, and H. Cheong, Ising-type magnetic ordering in atomically thin $FePS_3$, Nano Lett. 16, 7433 (2016).

[30] D. Lançon, H. C. Walker, E. Ressouche, B. Ouladdiaf, K. C. Rule, G. J. McIntyre, T. J. Hicks, H. M. Rønnow, and A. R. Wildes, Magnetic structure and magnon dynamics of the quasi-two-dimensional antiferromagnet $FePS_3$, Phys. Rev. B 94, 214407 (2016).

[31] A. McCreary, J. R. Simpson, T. T. Mai, R. D. McMichael, J. E. Douglas, N. Butch, C. Dennis, R. Valdés Aguilar, and A. R. Hight Walker, Quasi-two-dimensional magnon identification in antiferromagnetic $FePS_3$ via magneto-Raman spectroscopy, Phys. Rev. B 101, 064416 (2020).

[32] X. Qian, J. Liu, L. Fu, and J. Li, Quantum spin Hall effect in two-dimensional transition metal dichalcogenides, Science 346, 1344 (2014).

[33] J. H. Seol, I. Jo, A. L. Moore, L. Lindsay, Z. H. Aitken, M. T. Pettes, X. Li, Z. Yao, R. Huang, D. Broido et al., Two-dimensional phonon transport in supported graphene, Science 328, 213 (2010).

[34] A. Cepellotti, G. Fugallo, L. Paulatto, M. Lazzeri, F. Mauri, and N. Marzari, Phonon hydrodynamics in two-dimensional materials, Nat. Commun. 6, 6400 (2015).

[35] See Supplemental Material at http://link.aps.org/supplemental/10.1103/PhysRevLett.127.097401 for complete experimental details, full derivation, and details of the modeling, which includes Refs. [36–45].

[36] D. L. Rousseau, R. P. Bauman, and S. P. S. Porto, Normal mode determination in crystals, J. Raman Spectrosc. 10, 253 (1981).

[37] A. P. Cracknell, Scattering matrices for the raman effect in magnetic crystals, J. Phys. C 2, 500 (1969).

[38] S. Zhang, G. Go, K.-J. Lee, and S. K. Kim, Su(3) Topology of Magnon-Phonon Hybridization in 2D Antiferromagnets, Phys. Rev. Lett. 124, 147204 (2020).

[39] S. Park and B.-J. Yang, Topological magnetoelastic excitations in noncollinear antiferromagnets, Phys. Rev. B 99, 174435 (2019).

[40] G. Go, S. K. Kim, and K.-J. Lee, Topological Magnon-Phonon Hybrid Excitations in Two-Dimensional Ferromagnets with Tunable Chern Numbers, Phys. Rev. Lett. 123, 237207 (2019).

[41] P. Shen and S. K. Kim, Magnetic field control of topological magnon-polaron bands in two-dimensional ferromagnets, Phys. Rev. B 101, 125111 (2020).

[42] E. Callen and H. B. Callen, Magnetostriction, forced magnetostriction, and anomalous thermal expansion in ferromagnets, Phys. Rev. 139, A455 (1965).

[43] M. Boiteux, P. Doussineau, B. Ferry, and U. T. Höchli, Antiferroacoustic resonances and magnetoelastic coupling in $GdAlO_3$, Phys. Rev. B 6, 2752 (1972).

[44] W. E. Evenson and S. H. Liu, Theory of magnetic ordering in the heavy rare earths, Phys. Rev. 178, 783 (1969).

[45] S. L. Holm, A. Kreisel, T. K. Schäffer, A. Bakke, M. Bertelsen, U. B. Hansen, M. Retuerto, J. Larsen, D. Prabhakaran, P. P. Deen, Z. Yamani, J. O. Birk, U. Stuhr, C. Niedermayer, A. L. Fennell, B. M. Andersen, and K. Lefmann, Magnetic ground state and magnon-phonon interaction in multiferroic h-$YMnO_3$, Phys. Rev. B 97, 134304 (2018).

[46] A. Wildes, K. C. Rule, R. Bewley, M. Enderle, and T. J. Hicks, The magnon dynamics and spin exchange parameters of FePS$_3$, J. Phys. Condens. Matter **24**, 416004 (2012).

[47] A. Hashemi, H.-P. Komsa, M. Puska, and A. V. Krasheninnikov, Vibrational properties of metal phosphorus trichalcogenides from first-principles calculations, J. Phys. Chem. C **121**, 27207 (2017).

[48] D. Vaclavkova, A. Delhomme, C. Faugeras, M. Potemski, A. Bogucki, J. Suffczyński, P. Kossacki, A. R. Wildes, B. Grémaud, and A. Saúl, Magnetoelastic interaction in the two-dimensional magnetic material MnPS$_3$ studied by first principles calculations and Raman experiments, 2D Mater. **7**, 035030 (2020).

[49] In a collinear AFM with easy-axis anisotropy, symmetry permits doubly degenerate magnon modes, whose degeneracy can be lifted by magnetic field along the easy-axis [50,51].

[50] F. Keffer and C. Kittel, Theory of antiferromagnetic resonance, Phys. Rev. **85**, 329 (1952).

[51] P. A. Fleury and R. Loudon, Scattering of light by one- and two-magnon excitations, Phys. Rev. **166**, 514 (1968).

[52] M. Balkanski, M. Jouanne, and M. Scagliotti, Magnetic ordering induced Raman scattering in FePS$_3$ and NiPS$_3$ layered compounds, Pure Appl. Chem. **59**, 1247 (1987).

[53] K. Kim, S. Y. Lim, J. Kim, J. U. Lee, S. Lee, P. Kim, K. Park, S. Son, C. H. Park, J. G. Park, and H. Cheong, Antiferromagnetic ordering in van der Waals 2D magnetic material MnPS$_3$ probed by Raman spectroscopy, 2D Mater. **6**, 041001 (2019).

[54] G. Long, T. Zhang, X. Cai, J. Hu, C. W. Cho, S. Xu, J. Shen, Z. Wu, T. Han, J. Lin, J. Wang, Y. Cai, R. Lortz, Z. Mao, and N. Wang, Isolation and characterization of few-layer manganese thiophosphite, ACS Nano **11**, 11330 (2017).

[55] T. Satoh, S.-J. Cho, R. Iida, T. Shimura, K. Kuroda, H. Ueda, Y. Ueda, B. A. Ivanov, F. Nori, and M. Fiebig, Spin Oscillations in Antiferromagnetic NiO Triggered by Circularly Polarized Light, Phys. Rev. Lett. **105**, 077402 (2010).

[56] R. Cheng, S. Okamoto, and D. Xiao, Spin Nernst Effect of Magnons in Collinear Antiferromagnets, Phys. Rev. Lett. **117**, 217202 (2016).

[57] A. Rückriegel, S. Streib, G. E. Bauer, and R. A. Duine, Angular momentum conservation and phonon spin in magnetic insulators, Phys. Rev. B **101**, 104402 (2020).